Available online at www.sciencedirect.com
SCIENCE DIRECT®
International Journal of Heat and Fluid Flow 26 (2005) 530–546
International Journal of HEAT AND FLUID FLOW
www.elsevier.com/locate/ijhff

Heat transfer enhancement by using nanofluids in forced convection flows

Sidi El Bécaye Maïga [a], Samy Joseph Palm [a], Cong Tam Nguyen [a,*], Gilles Roy [a], Nicolas Galanis [b]

[a] Faculty of Engineering, Université de Moncton, Moncton, NB, Canada E1A 3E9
[b] Department of Mechanical Engineering, Faculty of Engineering, Université de Sherbrooke, Sherbrooke, Qc, Canada J1K 2R1

Accepted 7 February 2005
Available online 3 June 2005

Abstract

In the present paper, the problem of laminar forced convection flow of nanofluids has been thoroughly investigated for two particular geometrical configurations, namely a uniformly heated tube and a system of parallel, coaxial and heated disks. Numerical results, as obtained for water–γAl_2O_3 and Ethylene Glycol–γAl_2O_3 mixtures, have clearly shown that the inclusion of nanoparticles into the base fluids has produced a considerable augmentation of the heat transfer coefficient that clearly increases with an increase of the particle concentration. However, the presence of such particles has also induced drastic effects on the wall shear stress that increases appreciably with the particle loading. Among the mixtures studied, the Ethylene Glycol–γAl_2O_3 nanofluid appears to offer a better heat transfer enhancement than water–γAl_2O_3; it is also the one that has induced more pronounced adverse effects on the wall shear stress. For the case of tube flow, results have also shown that, in general, the heat transfer enhancement also increases considerably with an augmentation of the flow Reynolds number. Correlations have been provided for computing the Nusselt number for the nanofluids considered in terms of the Reynolds and the Prandtl numbers and this for both the thermal boundary conditions considered. For the case of radial flow, results have also shown that both the Reynolds number and the distance separating the disks do not seem to considerably affect in one way or another the heat transfer enhancement of the nanofluids (i.e. when compared to the base fluid at the same Reynolds number and distance).
© 2005 Elsevier Inc. All rights reserved.

Keywords: Laminar forced convection; Heat transfer enhancement; Heat transfer augmentation; Nanofluid; Nanoparticles; Tube flow; Radial flow

1. Introduction

Most conventional heat transfer fluids, such as water, Ethylene Glycol and engine oil, have limited capabilities in term of thermal properties, which in turn, may impose severe restrictions in many thermal applications. And in spite of considerable research and efforts deployed, a clear and urgent need does exist to date to develop new strategies in order to improve the effective thermal behaviours of these fluids. On the other hand, most solids, in particular metals, have thermal conductivities much higher, say by 1–3 orders of magnitude, compared to that of liquids. Hence, one can then expect that fluid containing solid particles may significantly increase its conductivity. Following the historical and pioneer work published hundred years ago by Maxwell (1904), numerous theoretical works (see in particular, Jeffrey, 1973; Batchelor, 1977; Gupte et al., 1995) and experimental studies (see for example, Boothroyd and Haque, 1970; Sohn and Chen, 1981; Kurosaki and Murasaki, 1986) have been conducted on liquids and gas containing suspended solid particles. In particular, research works performed for gas–solid particle flows—see for example,

* Corresponding author. Tel.: +1 506 858 4347; fax: +1 506 858 4082.
E-mail address: nguyenc@umoncton.ca (C.T. Nguyen).

0142-727X/$ - see front matter © 2005 Elsevier Inc. All rights reserved.
doi:10.1016/j.ijheatfluidflow.2005.02.004

Nomenclature

C_p	isobaric specific heat of the fluid
D	tube inside diameter
D_h	hydraulic diameter in radial flow, $D_h = 2R_i$
L	tube length
Nu	local Nusselt number, $Nu = hD/k_0$
$\overline{Nu}$	averaged Nusselt number = $\overline{h_{nf}}D/k_{nf}$
P	pressure
Pr	Prandtl number, $Pr = C_p\mu/k$
Q	volumetric flow rate
R or r	radial coordinate
Re	Reynolds number: $Re = \rho_0 V_0 D/\mu_{zero}$ for tube flow, $Re = 2Q/\pi R_i v_0$ for radial flow
R_{ext}	outer radius of the disks
R_i	radius of the inlet pipe
R_0	tube radius, $R_0 = D/2$
T	temperature
T_W	fluid temperature at the tube wall or on the heated disk wall
T_0	fluid inlet temperature (reference temperature)
Z	axial coordinate
V	velocity vector
V_R, V_θ, V_Z	radial, tangential and axial velocity component
V_0	uniform axial velocity at tube inlet
a	gap or channel height
h	local heat transfer coefficient
h_m or $\overline{h}$	averaged heat transfer coefficient
k	thermal conductivity of the fluid
q''_W	wall heat flux
r	radial coordinate
$\bar{r}$	normalised radial coordinate, $=r/R_i$

Greeks

α	thermal diffusivity
θ	tangential coordinate
μ	dynamic viscosity
ρ	density
τ	wall shear stress
$\bar{\tau}$	average wall shear stress
φ	volume concentration of particles

Subscripts

R, θ, Z	refer to the directions in space
W	refers to the wall condition
bf	refers to the base fluid
m	refers to the averaged value
nf	refers to the nanofluid
p	refers to the particles
r	refers to the 'nanofluid/base fluid' ratio
0	refers to the reference (inlet) condition

(Boothroyd and Haque (1970), Michaelides (1986), Kurosaki and Murasaki (1986), Murray (1994), Avila and Cervantes (1995) and Sato et al. (1998))—have shown that by adding small solid particles in gas, the heat transfer coefficient can considerably be augmented. For liquid–solid particle mixtures, significant heat transfer enhancement was also observed as well (Sohn and Chen, 1981; Ahuja, 1982). Such enhancement is due, in part, to the increase of the fluid effective thermal conductivity. On the other hand, it is believed that the reduction of the thermal boundary layer thickness due to the presence of particles and their random motion within the base fluid may have important contributions to such heat transfer improvement as well. One should note that the above mentioned studies were concerned with mixtures containing millimetre or micrometer size particles that have, unfortunately, introduced serious drawbacks such as drastic pressure drop, rapid settling of particles, severe clogging as well as premature wear of flow channels and its components. All of these difficulties have imposed severe limitation regarding the practical applications of such mixtures. In recent years, modern technologies have permitted the manufacturing of particles down to the nanometre scale, which have created a new class of fluids, called nanofluid.

The term 'nanofluid' refers to a two-phase mixture composed of a continuous phase, usually a saturated liquid, and a dispersed phase constituted of extremely fine metallic particles of size below 40 nm called 'nanoparticles'. It has been shown that the thermal properties of a nanofluid appear to be well higher than those of the base fluid. In fact, some available experimental data—see in particular, (Masuda et al., 1993; Choi, 1995; Lee et al., 1999)—have shown that even with a relatively low particle loading, say 1–5% in volume, the resulting mixture thermal conductivity may increase as much as 20% compared to that of the base liquid. Such an increase depends mainly on several factors such as the form and size of particles, the concentration and thermal properties of both constituents. Hence, nanofluids appear to be a very interesting alternative for advanced thermal applications, in particular micro-scale and nano-scale heat transfer, see for example Lee and Choi (1996). However, in spite of their great potentials and features, these rather special fluids are still in their early development. In fact, the first experimental works were mostly concerned with the determination of the effective thermal conductivity (Masuda et al., 1993; Choi, 1995; Pak and Cho, 1998; Lee et al., 1999; Wang et al., 1999; Eastman et al., 1999; Xuan and Li, 2000; Eastman

et al., 2001). Among these works, some have also provided data for the effective viscosity of nanofluids (Masuda et al., 1993; Pak and Cho, 1998; Wang et al., 1999). Wang et al. (2003) and Xuan et al. (2003) have studied the effect due to the particle clustering on the effective thermal conductivity by using fractal models. Most recently, Das et al. (2003) have experimentally investigated the influence of temperature on the nanofluid thermal conductivity. The above cited works considered current fluids such as water, Ethylene Glycol and engine oil containing metallic particles, γ-Al_2O_3, SiO_2, TiO_2, CuO and Cu particles. It should be noted that, with regard to the nanofluid thermal properties, the actual amount of experimental data available in the literature remains, surprisingly, quite small. Also, the influence of the particle shape on such properties has yet been clearly understood to date. It is obvious that more research works will be needed in this interesting issue in the near future.

From the theoretical viewpoint, it is important to mention that such a mixture of liquid and dispersed ultra-fine particles represents a new, very interesting yet a rather complex challenge to researchers in the domain of fluid mechanics and heat transfer, because of the fact that it appears very difficult, if not to say practically impossible, to formulate any theory that can reasonably predict the flow of nanofluid by considering it as a multi-component fluid (Drew and Passman, 1999). On the other hand, since a nanofluid is by nature a two-phase fluid, one can expect that it may possess some common features with the solid–fluid mixtures. On such an interesting issue, the question regarding the applicability of the theory of classical two-phase flows for nanofluids remains open. Also, due to the random movement and the extreme size of particles, one should mention some fascinating yet rather complex phenomena such as thermal dispersion, intermolecular energy exchange and liquid layering on the solid–liquid interface as well as phonon effects on the heat transport inside the particle itself. Such phenomena are under intensive investigations from researchers around the world to date, see for example, Keblinski et al. (2002) and Ohara and Suzuki (2000).

With regard to the thermal performance of nanofluids in confined flow situations, the only and recent experimental works by Pak and Cho (1998) and Li and Xuan (2002) have provided the first empirical correlation for computing the Nusselt number in both laminar and turbulent tube flow using nanofluids composed of water and Cu, TiO_2 and γ-Al_2O_3 particles. Results from these studies have clearly shown that the suspended nanoparticles have produced a remarkable increase of the heat transfer capability of the base fluid, and the nanofluids clearly give higher heat transfer coefficient than the base-fluid (saturated water) for a same Reynolds number. Such improvement becomes more important with an augmentation of the particle loading. Recent numerical results from the authors' studies (Maïga et al., 2004a,b; Palm et al., 2004; Roy et al., 2004) have clearly confirmed the superior thermal performance given by nanofluids, in particular Ethylene Glycol–γAl_2O_3 mixture, for use in different confined flow configurations. It is important to note that, to our knowledge, there is no available data regarding the radial flow of nanofluids in the literature.

In the present work, we have thoroughly studied the heat transfer enhancement and behaviours of nanofluids, namely water–γAl_2O_3 and Ethylene Glycol–γAl_2O_3 in two different confined flow situations. Some of the most complete and significant results will be presented and discussed in the following.

2. Mathematical modelling

2.1. Geometrical configurations and governing equations

Fig. 1a and b show the geometrical configurations under consideration. It consists of the steady, forced laminar convection flow and heat transfer of a nanofluid flowing inside (i) a straight tube of circular cross-section, *Case 1* and (ii) a radial channel between a pair of parallel, coaxial disks, *Case 2*. In *Case 1*, the fluid enters with uniform temperature and axial velocity profiles at the inlet section. The tube is long enough so that the fully developed flow conditions prevail at the outlet section. Both conditions of the axially and circumferentially uni-

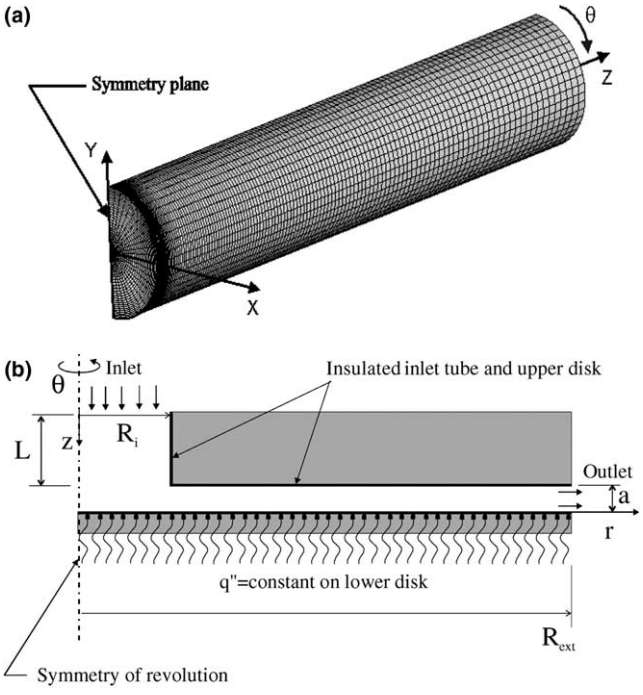

Fig. 1. Geometrical configurations under study: (a) a uniformly heated tube and (b) a radial channel between heated disks.

form wall heat flux and the constant wall temperature have been considered in this study. Also, the flow and the thermal field are assumed to be symmetrical with respect to the vertical plane passing through the tube main axis. In *Case 2*, the parallel and coaxial disks of outer radius R_{ext} are separated by a gap "a". The fluid is forced into the channel through an inlet orifice of radius R_i and exits at the disks periphery. On the impinged disk i.e. the lower disk, a constant heat flux q''_W is imposed throughout; the upper disk and inlet tube are assumed insulated.

2.1.1. Assumptions

As mentioned earlier, there exists no formulated theory to date that could reasonably predict the flow behaviours of a nanofluid by considering it as a multi-component material. It should be noted that most nanofluids used in practical applications of heat transfer purposes are usually composed of particles finer than 40 nm. Because of such extremely reduced dimension, it has been suggested that these particles may be easily fluidized and consequently, can be considered to behave more like a fluid (Xuan and Roetzel, 2000). Furthermore, by assuming negligible motion slip between the particles and the continuous phase, and the thermal equilibrium conditions also prevail, the nanofluid may be then considered as a conventional single-phase fluid with effective physical properties being function of the properties of both constituents and their respective concentrations (Pak and Cho, 1998; Xuan and Roetzel, 2000). An interesting result from such an assumption resides in the fact that an extension from a conventional fluid to a nanofluid appears feasible, and one may expect that the classic theory as developed for conventional single-phase fluids can be then applied to nanofluids as well. Thus, all the equations of conservation (mass, momentum and energy) as well known for single-phase fluids can be directly extended and employed for nanofluids. It is very interesting to mention that, although more experimental data will be needed in order to assess such an assumption, it seems to be validated, to some extent, through the recent experimental works in which correlation of the form similar to that of the well-known Dittus–Boelter formula have been proposed to characterize the heat transfer of nanofluids (Pak and Cho, 1998; Li and Xuan, 2002).

In the present work, in conjunction with the arguments stated above, we have adopted the 'single phase fluid' approach in order to be able to study the thermal behaviors of nanofluids. For the particular applications under consideration, we have assumed that the nanofluids are incompressible with constant physical properties. Also, both the compression work and viscous dissipation are assumed negligible in the energy equation.

Under such conditions, the general conservation equations written in the vector form are as follows (Warsi, 1999; Eckert and Drake, 1972):

- *Conservation of mass*

$$\mathrm{div}(\rho \mathbf{V}) = 0 \tag{1}$$

- *Conservation of momentum*

$$\mathrm{div}(\rho \mathbf{V}\mathbf{V}) = -\mathrm{grad}P + \mu \nabla^2 \mathbf{V} \tag{2}$$

- *Conservation of energy*

$$\mathrm{div}(\rho \mathbf{V} C_p T) = \mathrm{div}(k\,\mathrm{grad}\,T) \tag{3}$$

In the above equations, V, P and T are respectively fluid velocity vector, pressure and temperature; all fluid properties are evaluated at the reference temperature that is the fluid inlet temperature T_0.

2.2. Boundary conditions

The governing equations (1)–(3) constitute a highly non-linear and coupled equation system that must be solved subject to appropriate boundary conditions. For *Case 1* and at the tube inlet, profiles of uniform axial velocity V_0, temperature T_0 prevail. At the tube exit section, the fully developed conditions prevail, that is to say that all axial derivatives are zero. On the tube wall, the usual non-slip conditions are imposed; also, two different thermal boundary conditions have been considered in this study, namely the uniform wall heat flux and the uniform wall temperature condition. As noted earlier, both the flow and thermal fields are assumed symmetrical with respect to the vertical plane passing through the tube main axis. In *Case 2* for which it is assumed that the flow and the thermal field are axis-symmetrical, the usual non-slip conditions are also prescribed on all solid surfaces bounding the domain. The fluid has uniform axial velocity and temperature through its inlet port. On the impinged disk, a uniform heat flux q''_W is imposed, while the upper disk is assumed insulated. At the outlet section i.e. at $R = R_{ext}$, a known ambient pressure is imposed. A 'back-flow' fluid temperature has been specified as well for case where an inflow occurs through the outlet section.

2.3. Physical properties of the nanofluids

By assuming that the nanoparticles are well dispersed within the base-fluid i.e. the particle concentration can be considered uniform throughout the domain and, knowing the properties of the constituents as well as their respective concentrations, the effective physical properties of the mixtures studied can be evaluated using some classical formulas as well known for two-phase fluids. In the following equations, the subscripts 'p', 'bf' and 'nf' refer, respectively, to the particles, the base-fluid and the nanofluid, while 'r' refers to the 'nanofluid/base fluid' ratio of the physical quantity under consideration:

$$\rho_{nf} = (1-\varphi)\rho_{bf} + \varphi\rho_p \quad (4)$$

$$(C_p)_{nf} = (1-\varphi)(C_p)_{bf} + \varphi(C_p)_p \quad (5)$$

$$\mu_r = \frac{\mu_{nf}}{\mu_{bf}} = 123\varphi^2 + 7.3\varphi + 1 \quad \text{for water–}\gamma Al_2O_3 \quad (6)$$

$$\mu_r = \frac{\mu_{nf}}{\mu_{bf}} = 306\varphi^2 - 0.19\varphi + 1$$

$$\text{for Ethylene Glycol–}\gamma Al_2O_3 \quad (7)$$

$$k_r = \frac{k_{nf}}{k_{bf}} = 4.97\varphi^2 + 2.72\varphi + 1 \quad \text{for water–}\gamma Al_2O_3 \quad (8)$$

$$k_r = \frac{k_{nf}}{k_{bf}} = 28.905\varphi^2 + 2.8273\varphi + 1$$

$$\text{for Ethylene Glycol–}\gamma Al_2O_3 \quad (9)$$

Eqs. (4) and (5) are general relationships used to compute the density and specific heat for a classical two-phase mixture (see Pak and Cho, 1998). Eqs. (6) and (7) for computing the dynamic viscosity of nanofluids have been obtained by performing a least-square curve fitting of some scarce experimental data available for the mixtures considered (Masuda et al., 1993; Lee et al., 1999; Wang et al., 1999). The reason of such a choice resides in the fact that, although there exists some formulas such as the one proposed by Einstein and later improved by Brinkman (1952) as well as the one proposed by Batchelor (1977) that can be employed, it has been found that these formulas drastically underestimate the viscosity of the nanofluids under consideration with respect to the measured data, as shown by Maïga et al. (2004b). Regarding the thermal conductivity of the nanofluids, the same situation does exist. Thus, although there are some experimental data for the nanofluids studied, these data remain quite scarce and are limited to a low particle concentration; unfortunately, they also exhibit a relatively large dispersion (see in particular, Maïga et al., 2004b). It is very important to mention that the enhance mechanism on the thermal conductivity of nanofluids is still not clear, and there exist today, to our knowledge, no theoretical and/or empirical model that can adequately characterise such an enhancement. In the present study, we have introduced Eqs. (8) and (9) that have been obtained using the model proposed by Hamilton and Crosser (1962) and this, assuming spherical particles. Such a model, which was first developed based on data from several mixtures containing relatively large particles i.e. millimetre and micrometer size particles, is believed to be acceptable for use with nanofluids, although it may give underestimated values of thermal conductivity. This model has been adopted in this study because of its simplicity as well as its interesting feature regarding the influence of the particle form itself. Details and discussion regarding the procedure of computing the physical properties of nanofluids considered have been presented elsewhere (Maïga, 2004; Maïga et al., 2004b). It is important to mention that the data employed for the nanofluids considered were obtained at fixed reference temperatures, that is to say that the influence of the temperature on fluid thermal properties has yet been clearly established to date. Finally, for most of the nanofluids of engineering interest including the ones considered in the present study, the amount of experimental data providing information on their physical properties remain, surprisingly, rather scarce if not to say quasi-non-existing for some. Hence, much more research works will be, indeed, needed in this field.

2.4. Dimensionless governing parameters

One can determine that for *Case 1*, the problem of forced convection tube flow can be characterized by a set of five dimensionless parameters, namely the flow Reynolds number, $Re = V_0 D\rho/\mu$, the Prandtl number, $Pr = C_p\mu/k$, the particle volume concentration φ and the property ratios $\Gamma_1 = k_p/k_{bf}$ and $\Gamma_2 = (C_p)_p/(C_p)_{bf}$. For *Case 2*, it can be shown that the problem is governed by a set of seven dimensionless parameters, namely the through flow Reynolds number $Re = 2Q/\pi R_i v$, the Prandtl number Pr, the aspect ratios $\eta = a/R_i$ and $\beta = R_{ext}/R_i$, the particle concentration φ and the property ratios Γ_1 and Γ_2. It should be noted that the shape as well as the dimensions of the particles themselves also constitute factors that may have some influence on the heat transfer and fluid flow characteristics of the resulting nanofluid. Such effect has yet been clearly understood and further experimental works appear, in our opinion, a clear necessity.

3. Numerical method and code validation

The system of governing equations (1)–(3), subject to their appropriate boundary conditions for both cases, has been successfully solved by using the numerical method that is essentially based on the 'finite control volume approach'. Since such method has been very well documented elsewhere, see in particular Patankar (1980), only a brief review is given here. This method, as other members of the SIMPLE-code family, is based on the spatial integration of the conservation equations over finite control volumes. The power-law scheme was used throughout to compute the so-called 'combined convection-and-diffusion' fluxes of heat, momentum and other quantities resulting from the transport process. Also, the staggered grids have been used where the velocity components are calculated at the center of the volume interfaces while the pressure as well as other

scalar quantities such as fluid temperature are computed at the center of a control-volume. The algebraic 'discretized equations' resulting from this spatial integration process have been sequentially i.e. one at a time and iteratively solved throughout the physical domain considered, by combining the 'line-by-line' procedure, the well-known TDMA technique ('Three Diagonal Matrix Algorithm') and the efficient alternate-direction and multi-passes-sweeping technique. On the other hand, the special 'pressure-correction' equation, obtained by a judicious combination of the discretized form of the Navier–Stokes equation (2) and the corresponding one of the continuity equation (1), has been employed not only to calculate the guessed pressure field but also to correct the guessed velocities field during the calculation process in order to progressively satisfy all the discretized equations (the reader is advised to consult Patankar (1980) for complete details regarding the above numerical method and procedures). As convergence indicator, we have essentially based on the residuals that result from the integration of the conservation equations (1)–(3) over finite control-volumes. During the iterative calculation process, these residuals were constantly monitored and carefully scrutinized. For all of the simulations performed in this study, converged solutions were usually achieved with residuals as low as 10^{-8} (or less) for all the governing equations. As starting conditions, we have employed the velocity and temperature fields corresponding to the cases of forced flow without particles. For subsequent cases, converged solutions as obtained for a given value of φ were used as initial conditions.

3.1. Grid sensitivity study

In order to ensure the accuracy as well as the consistency of numerical results, several non-uniform grids have been submitted to an extensive testing procedure for each of the cases considered.

For *Case 1*, results as obtained for a particular test case (see Maïga, 2004; Maïga et al., 2004b) have shown that for the tube flow problem under consideration, the $32 \times 24 \times 155$ non-uniform grid appears to be satisfactory to ensure the precision of numerical results as well as their independency with respect to the number of nodes used. Such grid has, respectively, 32, 24 and 155 nodes along the radial, tangential (for θ covering 0–180°) and axial directions, with highly packed grid points in the vicinity of the tube wall and especially in the entrance region.

For *Case 2* in which the flow field is assumed axis-symmetrical, results from several test cases and different grids have shown that the 500×60 non-uniform grid appears to be appropriate for the problem under study since it gives accurate results but does not cost much in term of computational efforts. Such grid possess respectively 500 and 60 nodes along the radial and axial direction (see again Fig. 1b); the grid points are highly packed near the channel entrance region as well as in the vicinity of all boundaries of the domain (see Palm et al., 2004 for details).

3.2. Code validation

3.2.1. Case 1

The computer model has been successfully validated, at first, by comparing the results as obtained for the development of fluid axial velocity V_Z to the corresponding analytical and numerical data by others for the classical case of a developing laminar forced convection flow in a tube (Eckert and Drake, 1972). Such a comparison has shown a very good agreement (see in particular, Maïga et al., 2004b). Fig. 2a shows, for example, another comparison of results as obtained for the local Nusselt number with others' numerical and experimental data. Again, the agreement appears quite acceptable (complete details regarding these validation tests may be found in Maïga, 2004).

3.2.2. Case 2

There exist, to our knowledge, no experimental results regarding the case of the flow and heat transfer of nanofluids in a radial flow cooling systems. Therefore, in order to validate the computer model, we have had to compare our numerical results with available data obtained experimentally with conventional fluids. The first comparison has been performed by comparing the radial velocity profile as obtained for a particular test case and the corresponding experimental data from Szeri et al. (1983) for the classical problem of the laminar flow of water between two coaxial disks. The agreement can be qualified as very good (Palm et al., 2004). The second validation test has been carried out considering the laminar flow and heat transfer between two coaxial heated disks. Fig. 2b shows for example the comparison of numerical results as obtained for the local Nusselt number and the corresponding experimental data from Mochizuki and Yang (1986). For this case, the governing parameters are, respectively, $Re = 1756$, $Pr = 0.7$ (air), $R_i = 80$ mm, $R_{ext} = 217$, $a = 3.9$ mm i.e. $\beta = 2.7$ and $\eta = 0.05$, the applied wall heat flux varies along the disk radius according to the relation $q''_W = 10.846/R^2$. Again, the agreement between the results obtained by our model and experiments can be qualified as quite satisfactory.More details regarding the validation tests and discussion for *Case 2* may be found elsewhere (see Palm, 2004; Palm et al., 2004).

In light of the above validation tests, one can conclude with confidence about the appropriateness of the mathematical models as well as the reliability of the numerical method adopted.

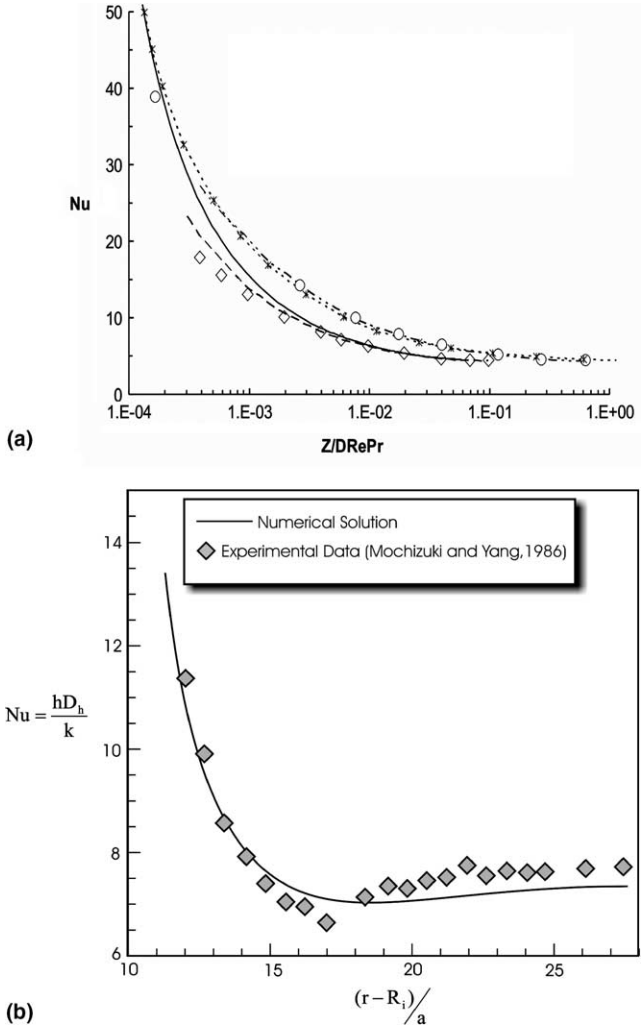

Fig. 2. Comparison with other results and experimental data for: (a) a forced convection tube flow heat transfer (◊ Petukhov et al., 1969; -- Orfi, 1995; — Present study; –·· Hornbeck, 1965; ○ Heaton et al., 1964; -*- Nguyen, 1988) and (b) heat transfer of a laminar air flow between heated disks.

4. Results and discussion

4.1. Results for Case 1: the laminar tube flow

We have performed extensive numerical simulations for *Case 1* considering two different nanofluids, namely water–γAl_2O_3 and Ethylene Glycol–γAl_2O_3. The heated tube has a diameter of 0.01 m and a total length of 1.0 m. For water–γAl_2O_3, the parameters are as follows: Re = 250, 500 and 1000; the wall heat flux q''_W has varied from 2500 W/m^2 to 15,000 W/m^2; and T_0 has been fixed to 293.15 K. On the other hand, for Ethylene Glycol–γAl_2O_3, simulations were carried out for the following parameters: Re = 6.31, 63.1 and 631; q''_W varies from 2500 W/m^2 to 5000 W/m^2; T_0 was fixed to 280 K for all cases performed. Numerical simulations were also carried out for the second thermal boundary condition for which a constant wall temperature of T_W = 363.15 K has been imposed for both fluids considered.

In the following, some significant results showing the beneficial influence of nanoparticles are presented and discussed; unless otherwise noted, most of the results presented are for water–γAl_2O_3 nanofluid with Re = 500 and $q''_W = 10,000$ W/m^2.

4.1.1. Effect of the particles concentration on the thermal field and wall shear stress

Results have revealed that the presence of nanoparticles has considerable effects on the thermal characteristics of the mixture. Fig. 3a shows the influence of the particle volume concentration φ on the radial temperature profile at the particular axial position Z = 0.95 m near the tube exit. One can observe that fluid temperatures have clearly decreased with an increase of the parameter φ, in particular in the vicinity of the tube wall, indicating that higher heat transfer rate with nanoparticles can then be achieved. Also, in the core region, there is a clear existence of a uniform temperature fluid

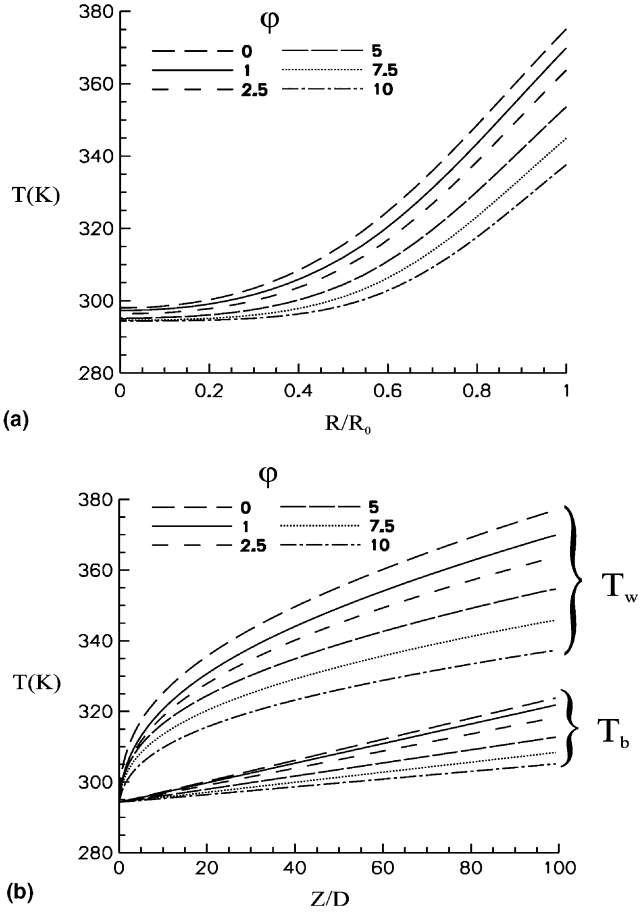

Fig. 3. Effect of parameter φ in tube flow: (a) fluid temperature profiles at Z = 0.95 m and (b) axial development of fluid bulk and wall temperature.

zone that becomes more visible for higher value of φ. Such behavior may be better understood by scrutinizing Fig. 3b where one can remark, for the axial position considered, a diminution of almost 37 K of the wall temperature between the case $\varphi = 10\%$ and the one without particles. It is interesting to note that such decrease of fluid temperature at the tube wall does exist all along the tube length and seems to be more important toward the exit. On the other hand, we can clearly observe that fluid bulk temperatures also decrease appreciably with the augmentation of particle loading. These results have obviously indicated the beneficial effects due to the nanoparticles, effects that may be explained by the fact that with the presence of such particles, the thermal properties of the resulting mixture have, in fact, become considerably more important. For a specific value of $\varphi = 7.5\%$ for example, it has been found that the values of the product ρC_p and the thermal conductivity k have increased as much as 14.2% and 23%, respectively, with respect to those corresponding to the case $\varphi = 0$. The nanofluid offers, as one may expect, higher thermal capability than the base (conventional) fluid. It can also be noted that with higher thermal conductivity of the mixture, the wall-to-fluid heat transfer would be, consequently, more important as we can see in the following results.

Fig. 4a shows that the use of nanofluid has, in fact, produced a considerable improvement of the heat transfer at the tube wall. Thus, for the particular value $\varphi = 7.5\%$ for example, the nanofluid-to-base fluid ratio h_r of convective heat transfer coefficients (h_r is defined as $h_r = h_{nf}/h_{bf}$) is approximately 1.63 near the tube end, that is to say, the heat transfer coefficient has increased by 63% over that of the base fluid (saturated water). Such ratio h_r clearly increases with an increase of the parameter φ, behaviour that is consistently observed over a major portion of the tube length. One can also observe that within a very short distance, say a few diameters, from the tube inlet, the ratio h_r appears clearly more important, but it decreases rather rapidly with the axial coordinate. Over the rest of the tube length, h_r remains nearly constant, except for low particle concentrations for which it slightly increases toward the tube end.

Regarding the wall shear stress, numerical results have shown, however, that the inclusion of nanoparticles into a base liquid has caused a drastic effect upon it. Fig. 4b shows the axial development of the nanofluid-to-base fluid ratio τ_r (defined as $\tau_r = \tau_{nf}/\tau_{bf}$) for the case $Re = 500$ and various particle concentrations. One can observe, at first, that for a given value of the parameter φ, this ratio τ_r appears mostly constant over the tube length, with an exception of a very short distance from the tube inlet (not visible on the figure). In general, τ_r increases considerably with the particle volume fraction φ, and this consistently along the tube

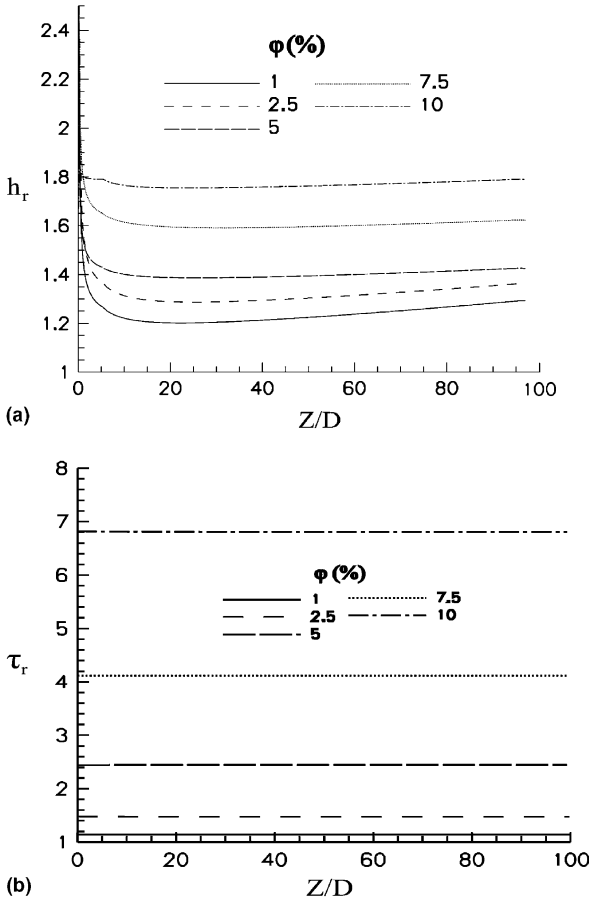

Fig. 4. Effect of parameter φ on axial development of (tube flow): (a) heat transfer coefficient ratio h_r and (b) wall shear stress ratio τ_r.

length. For the specific value $\varphi = 7.5\%$ for example, τ_r has a value of 4.11 i.e. the wall shear stress is now quadruple of that corresponding to the base fluid given identical operating conditions. Complete results obtained in the present study have shown that similar behaviors were also observed for other cases with different Reynolds number as well as for the other nanofluid considered in this study, Ethylene Glycol–γAl_2O_3. These adverse effects are somewhat expected as they obviously result from an important increase of the mixture viscosity due to the inclusion of nanoparticles. In fact, for water–γAl_2O_3 nanofluid in particular, its effective dynamic viscosity is almost multiplied by a factor of 2.24 for the case $\varphi = 7.5\%$ with respect to that of the base fluid (i.e. $\varphi = 0$); the corresponding multiplicative factor nearly reaches 2.71 for Ethylene Glycol–γAl_2O_3 mixture.

Complete results as obtained for other cases considering water–γAl_2O_3 and Ethylene Glycol–γAl_2O_3 mixtures and different values of the flow Reynolds number have also shown similar behaviors regarding the beneficial effects on the heat transfer as well as on the adverse ones observed previously on the wall shear stress due to the

inclusion of nanoparticles within the base fluids (Maïga, 2004).

4.1.2. Effect of the particles concentration and the flow Reynolds number on the averaged heat transfer for water–γAl_2O_3 mixture

In the present study, we are also interested to establish, on the average basis, the overall influence of nanoparticles on both the heat transfer and the wall shear stress. Fig. 5a–c show, respectively, the global effects due to the inclusion of particles on the averaged heat transfer coefficient $\bar{h}$, the averaged heat transfer coefficient ratio $\overline{h_r}$ and the averaged Nusselt number $\overline{Nu}$ for water–γAl_2O_3 mixture (note that the coefficient $\bar{h}$ is the surface-averaged value calculated on the entire tube length; $\overline{h_r}$ is defined as the nanofluid-to-base fluid ratio of the averaged heat transfer coefficients, $\overline{h_r} = \overline{h_{nf}}/\overline{h_{bf}}$). The averaged Nusselt number $\overline{Nu}$ is defined as $\overline{Nu} = \overline{h_{nf}}D/k_{nf}$ for nanofluids and $\overline{Nu} = \overline{h_{bf}}D/k_{bf}$ for a base fluid). It is interesting to observe, at first, from Fig. 5a, that the previously discussed beneficial effects due to nanoparticles do always exist regardless the flow Reynolds number. For a given value of *Re*, the averaged heat transfer coefficient $\bar{h}$ clearly increases with the increase of the parameter φ. Thus, for $Re = 250$ for example, $\bar{h}$ has increased almost by 32%, from 342 W/m^2 K ($\varphi = 0$) to 491 W/m^2 K ($\varphi = 10\%$). Such enhancement appears more important for a higher Reynolds number; for $Re = 1000$ in particular, the corresponding values of $\bar{h}$ are 510 W/m^2 K and 1054 W/m^2 K for the same values considered of φ, thus an augmentation of nearly 107% of the averaged heat transfer coefficient. On the other hand, for a given value of particle concentration φ, one can observe that the heat transfer enhancement also becomes considerably more important with the increase of the Reynolds number. Thus, for $\varphi = 7.5\%$ for example, $\bar{h}$ has as values, 466 W/m^2 K, 653 W/m^2 K and 900 W/m^2 K, respectively, for $Re = 250$, 500 and 1000. For lower particle loadings, say for $\varphi = 1\%$ in particular, such heat transfer enhancement, although remained interesting, appears less pronounced; in fact, $\bar{h}$ has augmented by only 50% for *Re* increasing from 250 to 1000.

All of these interesting behaviors have also been observed as well on Fig. 5b and c that present the dependence of the heat transfer coefficient ratio $\overline{h_r}$ as well as of the averaged Nusselt number $\overline{Nu}$ with respect to the governing parameters *Re* and φ. The ratio $\overline{h_r}$ is particularly interesting since it indicates the degree of heat

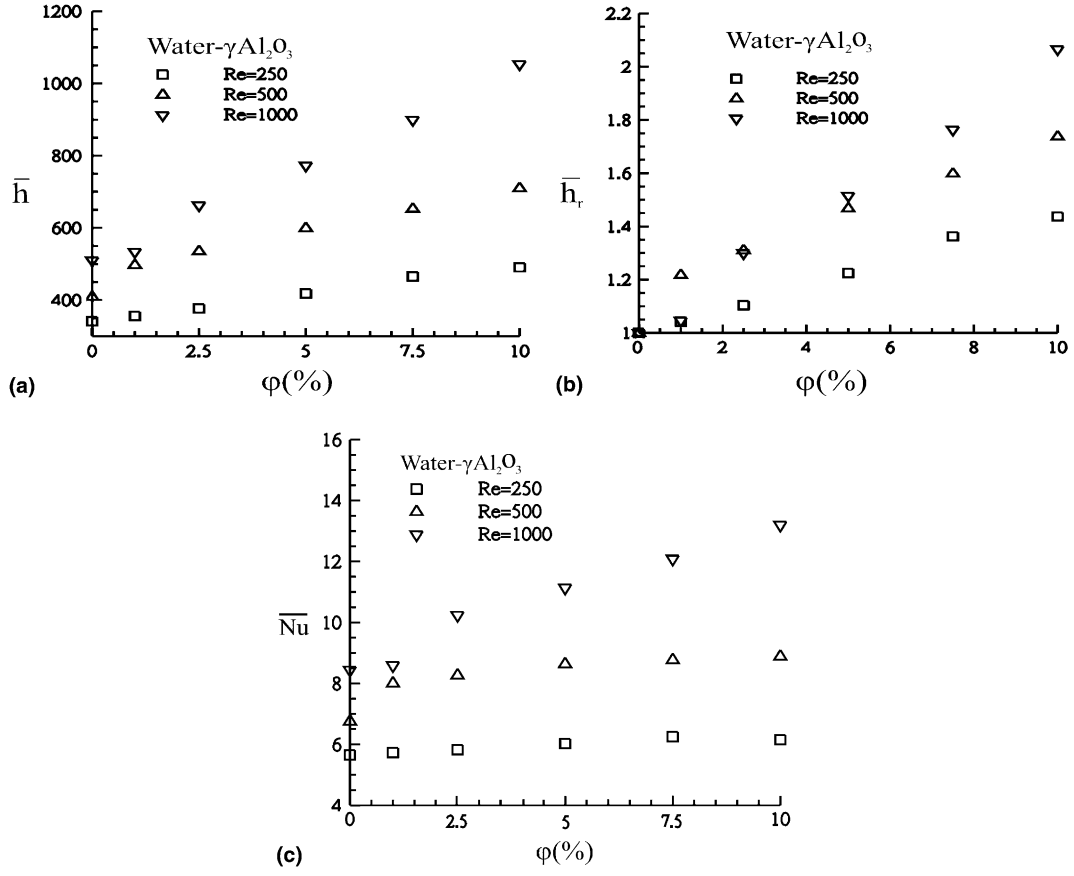

Fig. 5. Influence of parameters *Re* and φ for water–γAl_2O_3 mixture on tube flow: (a) averaged heat transfer coefficient, (b) averaged heat transfer coefficient ratio and (c) averaged Nusselt number.

transfer enhancement while compared to the base fluid. Here again, we can clearly observe from Fig. 5b that $\overline{h_r}$ increases considerably with the augmentation of either Reynolds number or particle loading parameter φ. Thus, for Re fixed at 1000, $\overline{h_r}$ has as values, 1.05, 1.30, 1.51, 1.76 and 2.07 respectively for $\varphi = 1\%$, 2.5%, 5%, 7.5% and 10%, that is to say that the averaged heat transfer coefficient has increased by 5%, 30%, 51%, 76% and 107% with respect to that of the base fluid (saturated water). For lower Re number, $\overline{h_r}$, although being always superior than 1, appears less important. On the other hand, for fixed value of φ, say $\varphi = 7.5\%$ for example, $\overline{h_r}$ has as values, 1.36, 1.60 and 1.76 respectively for $Re = 250$, 500 and 1000. For low particle concentrations however, the corresponding increase of $\overline{h_r}$ with respect to the parameter Re appears to be less pronounced. With regard to the dependence of the averaged Nusselt number with respect to the parameters Re and φ for water–γAl_2O_3 mixture, Fig. 5c, similar behaviours have been observed. For φ varying from 0% to 10%, $\overline{Nu}$ has increased from 5.65 to 6.15 for $Re = 250$, from 6.76 to 8.89 for $Re = 500$ and from 8.44 to 13.20 for $Re = 1000$. We also observe that for the cases with a low Reynolds number, say for $Re = 250$ in particular, the increase of $\overline{Nu}$ with respect to the particle loading parameter φ appears less pronounced than that found for other values of Re. One should note here that the definition of $\overline{Nu}$ includes k_{nf}, which also increases appreciably with an augmentation of the particle concentration φ; hence an appreciable increase of the averaged heat transfer coefficient $\overline{h}$ does not necessarily reflect in the value of $\overline{Nu}$.

Finally, although a direct comparison with others' results and experimental data was not possible due to a clear lack of data for water–γAl_2O_3 mixture in laminar tube flow, it is very interesting to mention that the above results regarding the heat transfer enhancement due to nanoparticles as well as the dependence of such enhancement with respect to the particle volume concentration and the flow Reynolds number, have been found to be consistent with the experimental data and trends observed for a mixture composed of saturated water and copper particles under laminar flow regime in a tube (see in particular Li and Xuan, 2002).

4.1.3. Effect of the particles concentration and the flow Reynolds number on the averaged heat transfer for Ethylene Glycol–γAl_2O_3 nanofluid

On the average basis, the overall influence of nanoparticles on both the heat transfer and the wall shear stress has also been investigated for Ethylene Glycol–γAl_2O_3 mixture as well. In the following, some significant results as obtained for $Re = 6.31$, 63.1 and 631 and $q''_W = 5000\ W/m^2$ are presented and discussed. Fig. 6a–c show, respectively, the global effects due to the inclusion of nanoparticles on the dependent variables $\bar{h}$, $\overline{h_r}$ and $\overline{Nu}$. We can notice, here again, similar behaviors regarding the influence of the governing parameters Re and φ. Thus, for a relatively low Re, say for $Re = 6.31$ for example, $\bar{h}$ has increases from 179 W/m^2 K ($\varphi = 0$) to 316 W/m^2 K ($\varphi = 10\%$). For higher Reynolds numbers, a value of $\bar{h}$ as high as 5594 W/m^2 K can then be achieved ($Re = 631$ and $\varphi = 10\%$). The increase of heat transfer with respect to the base fluid may be better understood by scrutinizing Fig. 6b. Thus, for $Re = 6.31$ in particular, the ratio $\overline{h_r}$ has as values, 1.04, 1.11, 1.26, 1.48 and 1.76, respectively for $\varphi = 1\%$, 2.5%, 5%, 7.5% and 10%. For higher Reynolds number, such increase of $\overline{h_r}$ with respect to the parameter φ appears more important. Thus, values of $\overline{h_r}$ as high as 2.39 ($Re = 63.1$) and 2.73 ($Re = 631$) have been achieved with $\varphi = 10\%$. It is very interesting to note that for relatively low particle loading, say for $\varphi < 2.5\%$, $\overline{h_r}$ is nearly identical for the Reynolds numbers considered, behavior that was not observed for water–γAl_2O_3 mixture. On the other hand, one can also observe that the increase of $\overline{h_r}$ with respect to the parameter Re becomes more pronounced only for moderate to high particle concentrations, say for $\varphi \geqslant 5\%$. For the ranges of the governing parameters studied in this study and by considering the values of $\overline{h_r}$, one may say that the heat transfer enhancement appears more important for Ethylene Glycol–γAl_2O_3 than for water–γAl_2O_3 mixture. Finally, for the cases studied considering Ethylene Glycol–γAl_2O_3, the averaged Nusselt number $\overline{Nu}$ has increased from 6.00 to 6.74 ($Re = 6.31$), from 13.63 to 20.72 ($Re = 63.1$) and from 68.61 to 119.20 ($Re = 631$) for φ varying from 0 to 10%. As previously observed for the case of water–γAl_2O_3 mixture, we may see, here again, that the increase of $\overline{Nu}$ with respect to the parameter φ appears to be low for $Re = 6.31$, but for higher Reynolds number, say for $Re = 631$, such increase has become very pronounced.

4.1.4. Correlations for $\overline{Nu}$

It is interesting to note that, although the results are not shown in the present paper for the sake of space, similar behaviors regarding the beneficial effect due to nanoparticles have also been observed as well in the case of the constant wall temperature boundary condition (see Maïga, 2004 for complete results and discussion).

From the numerical results obtained for the tube flow and the nanofluids considered, the following correlations have been proposed for computing the averaged Nusselt number $\overline{Nu}$ as function of the governing parameters Re and Pr:

$$\overline{Nu} = 0.086 Re^{0.55} Pr^{0.5} \quad \text{for constant wall heat flux} \tag{10}$$

$$\overline{Nu} = 0.28 Re^{0.35} Pr^{0.36} \quad \text{for constant wall temperature} \tag{11}$$

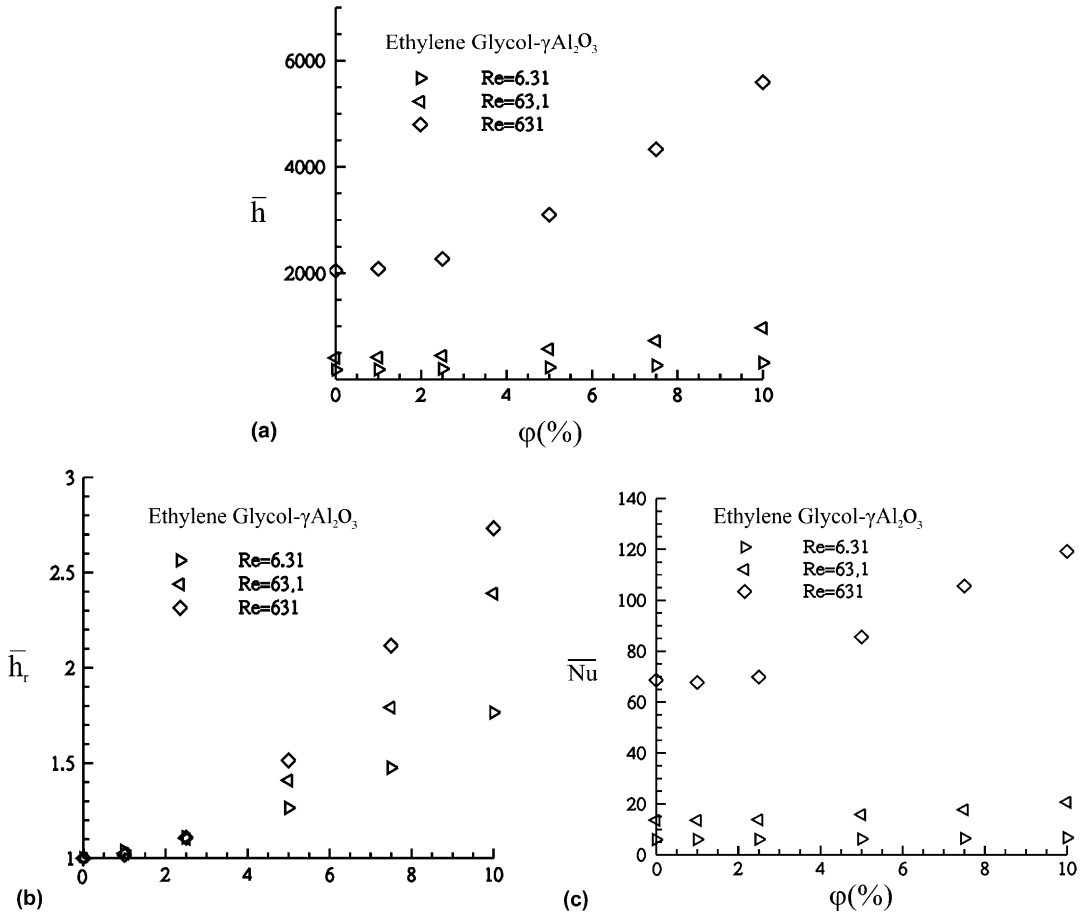

Fig. 6. Influence of parameters *Re* and φ for Ethylene Glycol–γAl_2O_3 mixture on (tube flow): (a) averaged heat transfer coefficient, (b) averaged heat transfer coefficient ratio and (c) averaged Nusselt number.

For the above correlations, the values of the maximum, RMS and standard deviation of the relative errors are, respectively, 28%, 13.8% and 8% for Eq. (10) and 19.5%, 7.3% and 6.8% for Eq. (11), errors that appear, in our opinion, quite reasonable. The correlations are valid for the following ranges of the parameters *Re*, *Pr* and φ, namely $Re \leqslant 1000$, $6 \leqslant Pr \leqslant 753$ and $\varphi \leqslant 10\%$. They are believed to be among the first of their kind.

4.1.5. Effect of the particles concentration and the flow Reynolds number on the averaged wall shear stress

Fig. 7 shows finally the dependence of the nanofluid-to-base fluid ratio $\overline{\tau_r}$, defined as the ratio of the averaged wall shear stresses $\overline{\tau_r} = \overline{\tau_{nf}}/\overline{\tau_{bf}}$, with respect to the particle loading parameter φ and the flow Reynolds number (here again, the quantities $\overline{\tau_{nf}}$ and $\overline{\tau_{bf}}$ are surface-averaged values that have been calculated over the entire tube length). For both nanofluids under study, it is interesting to observe, as one may expect, that the averaged wall shear stress has considerably increased with an augmentation of φ. Thus, for water–γAl_2O_3 mixture and

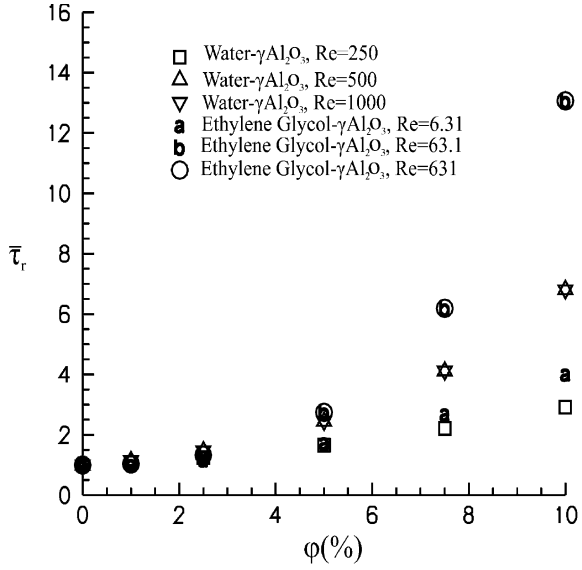

Fig. 7. Influence of *Re* and φ on averaged shear stress ratio $\overline{\tau_r}$ in tube flow.

$Re = 250$ in particular, $\overline{\tau_r}$ has as values, 1.08, 1.25, 1.66, 2.21 and 2.92 respectively for $\varphi = 1\%$, 2.5%, 5%,

7.5% and 10%. For higher Reynolds number, the corresponding increase of $\overline{\tau_r}$ appears to be more pronounced; thus, for $Re = 500$ for example, $\overline{\tau_r}$ has jumped from 1.14 for $\varphi = 1\%$ to 6.81 for $\varphi = 10\%$. It is very interesting to note that for a given value of φ, the values of $\overline{\tau_r}$ are nearly identical for the cases $Re = 500$ and $Re = 1000$. Similar behaviors have also been observed for Ethylene Glycol–γAl_2O_3 nanofluid. Thus, for $Re = 6.31$ for example, $\overline{\tau_r}$ has as values, 1.03, 1.19, 1.76, 2.71 and 4.03 respectively for $\varphi = 1\%$, 2.5%, 5%, 7.5% and 10%; on the other hand, for $Re = 63.1$, $\overline{\tau_r}$ has jumped from 1.04 for $\varphi = 1\%$ to as much as 13.07 for $\varphi = 10\%$. Here again, we can see that for a given value of φ, $\overline{\tau_r}$ remains almost the same for cases $Re = 63.1$ and $Re = 631$. From the above values of $\overline{\tau_r}$ obtained and shown in Fig. 7, one may say that the increase of the wall shear stress with respect to the particle concentration φ appears to be considerably more important for Ethylene Glycol–γAl_2O_3 than for water–γAl_2O_3 mixture. In other words, the adverse effects induced by the presence of nanoparticles within a base fluid appear more drastic in the case of Ethylene Glycol–γAl_2O_3 nanofluid. Such behavior can be explained by the fact that given a same particle volume concentration φ that is sufficiently high, say $\varphi > 2.5\%$, the increase of the effective dynamic viscosity (with respect to the base fluid) is generally more important for Ethylene Glycol–γAl_2O_3 than for water–γAl_2O_3 nanofluid. Thus, for $\varphi = 7.5\%$ for example, we can determine from Eqs. (6) and (7) that such an increase is approximately 171% and 124%, respectively, for the first and the second mixture. Finally, regarding the dependence of $\overline{\tau_r}$ with respect to the flow Reynolds number, one can see that $\overline{\tau_r}$ also increases appreciably with an augmentation of Re. Such increase appears remarkably more pronounced for moderate to high particle concentrations. For the range of the Reynolds number considered, it is observed that the above adverse effects on the wall shear stress also appear more important for Ethylene Glycol–γAl_2O_3 than for water–γAl_2O_3 mixture.

4.2. Results for Case 2: the radial flow

For the case of radial flow under study, an extended numerical simulation has also been performed for both nanofluids considered, water–γAl_2O_3 and Ethylene Glycol–γAl_2O_3. Unless otherwise specified, the results presented hereafter are for $Re = 1500$, $R_i = 1.634 \times 10^{-2}$m, $R_{ext} = 0.15$ m and $a = 3.175 \times 10^{-3}$ m i.e. $\beta = 8.86$ and $\eta = 0.187$, $T_0 = 293.15$ K and uniform heat flux $q''_W = 10,000$ W/m^2. The bulk of the results are presented for the water–γAl_2O_3 nanofluid. For cases studying the effects of the Reynolds number as well as those of the distance separating the disks, a particle volume fraction of 5% has been chosen.

4.2.1. Effect of particle concentration on heat transfer and thermal fields

As we are primarily interested in quantifying the heat transfer enhancement benefits of nanofluids, Fig. 8a shows, at first, the relative increase of the average of the heat transfer coefficient as a function of the nanoparticle volume fraction φ for the nanofluids considered ($\overline{h_r}$ is defined as the ratio $(h_m)_{nf}/(h_m)_{bf}$ where the quantities $(h_m)_{nf}$ and $(h_m)_{bf}$ are both surface-averaged values that have been calculated over the entire area of the heated disk). As one can notice, significant heat transfer increases can be found with the use of suspended nanoparticles. For example, for water–γAl_2O_3 nanofluid with a volume fraction of nanoparticles of 7.5%, a 45% increase in the average wall heat transfer coefficient is found for a same Reynolds number. In the case of Ethylene Glycol–γAl_2O_3, the average wall heat transfer coefficient has a 70% increase for a volume fraction of 7.5%. We can even see that a two-fold increase would be possible for $\varphi = 10\%$. Comparing results for the two nanofluids, we can easily see that the Ethylene Glycol–γAl_2O_3 nanofluid gives better heat transfer enhancement compared to the water–γAl_2O_3 nanofluid. It is also interesting to note that for $\varphi \leqslant 5\%$, both nanofluids exhibit essentially the same heat transfer enhancement.

The effects of particle volume fraction on the heat transfer and thermal fields can also be seen on Fig. 8b and c, depicting respectively the local Nusselt number and the normalised disk wall temperature as functions of the radial position on the impinged disk for water–γAl_2O_3 nanofluid. In this case, the following definitions are used:

$$Nu = \frac{hD_h}{k} \tag{12}$$

where $D_h = 2R_i$ and $h = \frac{q''_W}{T_W - T_0}$.

In this last equation, T_W and T_0 are respectively the heated disk wall temperature and the reference temperature (i.e. fluid temperature at inlet). As it can be seen on Fig. 8b, the local Nusselt number clearly increases with the particle volume fraction. The general behaviour of the local Nusselt number with the radial position is well respected in this case. It can be observed, at first, that within the inlet region i.e. for $\bar{r} \leqslant 1$, the Nusselt number is generally more important and it increases considerably with the radial direction. Such behaviour is due to the combined effect of the impingement and the fluid acceleration along the heated disk, fluid that is still at a temperature close to that at the inlet section. On the other hand, the decrease of the Nusselt number with respect to the radial coordinate in the vicinity of $\bar{r} = 0$ is obviously due to the stagnation effect. We also observe the existence of the peaks around $\bar{r} = 1.25$, which can be explained by the localised flow acceleration around this location. In fact, as we will see later, a recirculation flow cell does exist and in this area and is

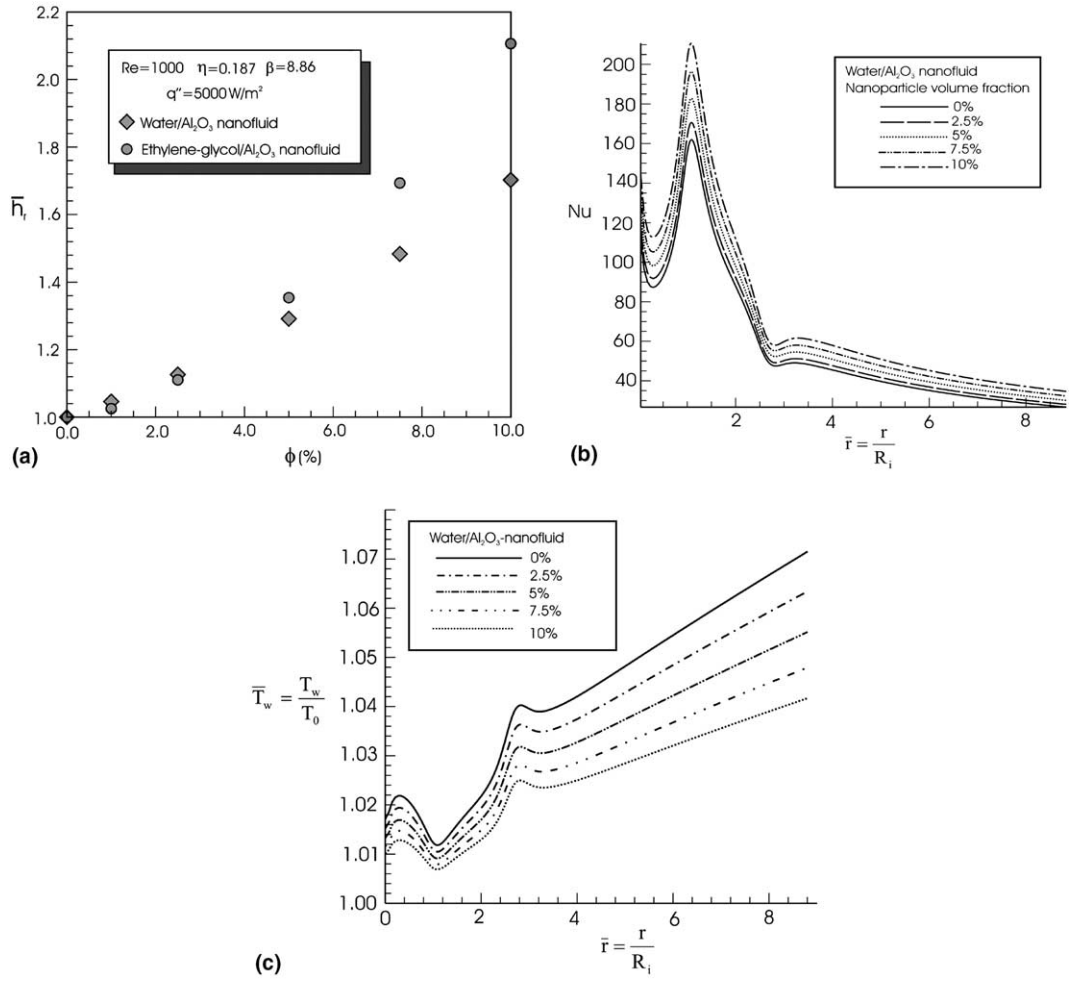

Fig. 8. Effect of particle loading parameter φ in radial flow: (a) averaged heat transfer coefficient ratio, (b) radial development of local Nusselt number and (c) radial development of local wall temperature.

attached to the opposite disk, which has induced a local acceleration of the fluid in channel. As a consequence, an increase of heat transfer results on the heated disk. For farther downstream i.e. radially outwards, a gradual flow deceleration decreases the local Nusselt number with the radial position. Fig. 8c shows the local wall temperature as a function of the radial position. For a given constant wall heat flux, we can see that an increase in the particle volume fraction decreases the local wall temperature, thus indicating obviously a better heat transfer performance at the surface. As it could be expected, the lowest temperatures found on the impinged disk are found at the point of locally accelerated flow (i.e. $\bar{r} \approx 1.0$–1.2 range).

4.2.2. Effect of Reynolds number on heat transfer

The influences of the through flow Reynolds number on heat transfer and hydrodynamic characteristics are presented in this section. Fig. 9a illustrates the influence of the Reynolds number on the local Nusselt number at the wall along the impinged disk. As it could be expected, the augmentation of the Nusselt number are found with an increase of *Re*. For Reynolds numbers below 1000, the same general distribution pattern as presented earlier (see again Fig. 8b) has been observed, with only differences in magnitude found between cases. However, for cases where *Re* are greater than 1000, we have observed changes not only in the magnitude but also in the radial variation of the Nusselt number as well. Such interesting behaviour can be explained by scrutinizing the corresponding hydrodynamic fields near the inlet region, Fig. 9b. Indeed, one can see that for $Re = 1500$ for example, only one recirculation cell is found (as discussed in the previous section, Fig. 8b) but for $Re = 2000$, a second recirculation cell is clearly observed on the impinged disk. It is interesting to note that the formation of the second recirculation cell has also been observed experimentally in the past, see for example McGinn (1956). Such changes in the localised flow conditions are the cause of changes in the Nusselt number profiles. In fact, the sudden drop of *Nu* for the case $Re = 2000$ (Fig. 9a) corresponds to the forma-

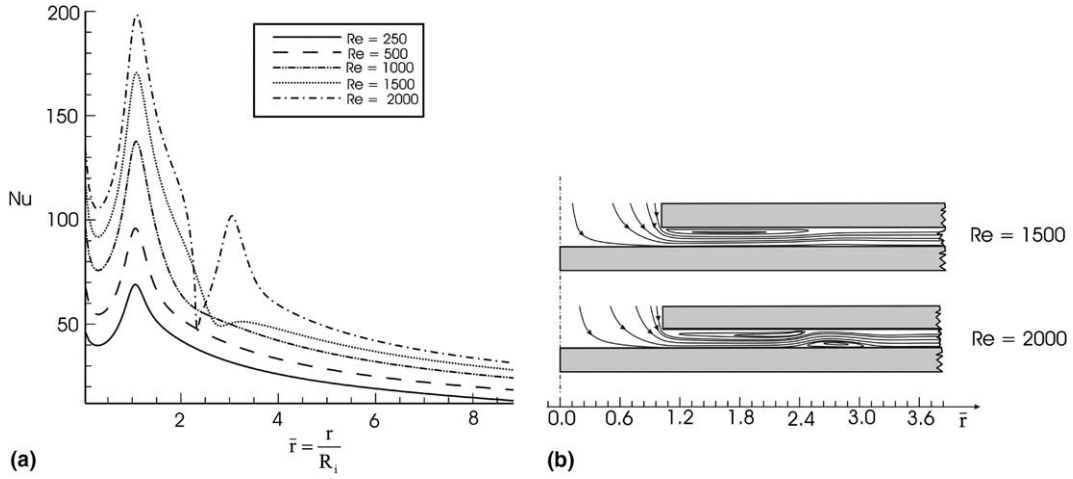

Fig. 9. Effect of through flow Reynolds number in radial flow: (a) radial development of local Nusselt number and (b) hydrodynamic field in the entrance region.

tion of a separated flow cell on the surface of the impinged disk. As the flow reattaches to the impinged disk, a second peak of the Nusselt number is then observed.

The combined effects of flow Reynolds number and particle concentration on the average heat transfer coefficient on the impinged disk are found in Fig. 10a. As it can be seen and as previously discussed, the general effect is a clear increase of the average heat transfer coefficient h_m with the increase of Re and φ. Of particular interest, however, is when h_m of the nanofluid is normalised by the corresponding h_m of the base fluid (for a same Re), the distribution illustrated in Fig. 10b is found. We can also observe that for the ranges of Re and φ considered, the global heat transfer enhancement seems relatively unaffected by the Reynolds number.

4.2.3. Effects of distance between disks on heat transfer

Another geometrical property which will undoubtedly affect the heat transfer in any radial flow cooling system is the distance separating the disks. Fig. 11a illustrates such effects (note that for the case shown, $Re = 500$ and $q''_W = 15,000\ W\ m^{-2}$). One can observe that as the distance separating the disks increases, a corresponding decrease in the Nusselt numbers is found. This behaviour, which is a direct consequence of the flow deceleration resulting of the increase of the gap between disks, appears consistent with other results for confined radial flows published in the literature (see for example Palm et al., 2004).

The overall heat transfer characteristics in this case can be presented in the form of the averaged heat transfer coefficient as a function of the particle volume fraction as well as of the distance separating the disks, Fig. 11b. As expected, an increase in the particle volume fraction and/or a decrease in the distance separating the disks will increase the averaged heat transfer coefficient. It is also interesting to observe that the influence of the particle loading parameter φ appears clearly more

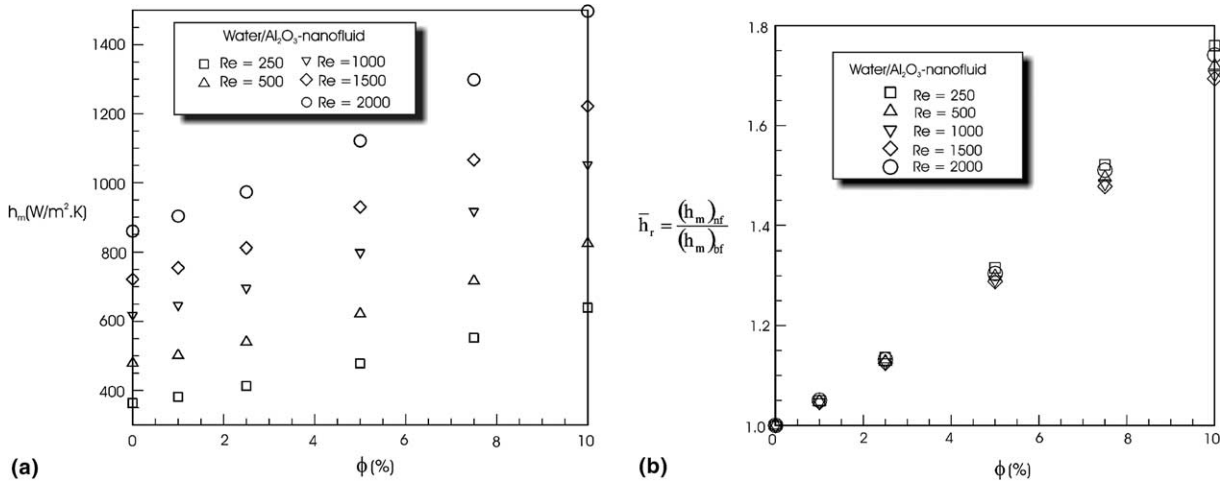

Fig. 10. Effect of parameters Re and φ in radial flow: (a) averaged heat transfer coefficient and (b) averaged heat transfer coefficient ratio.

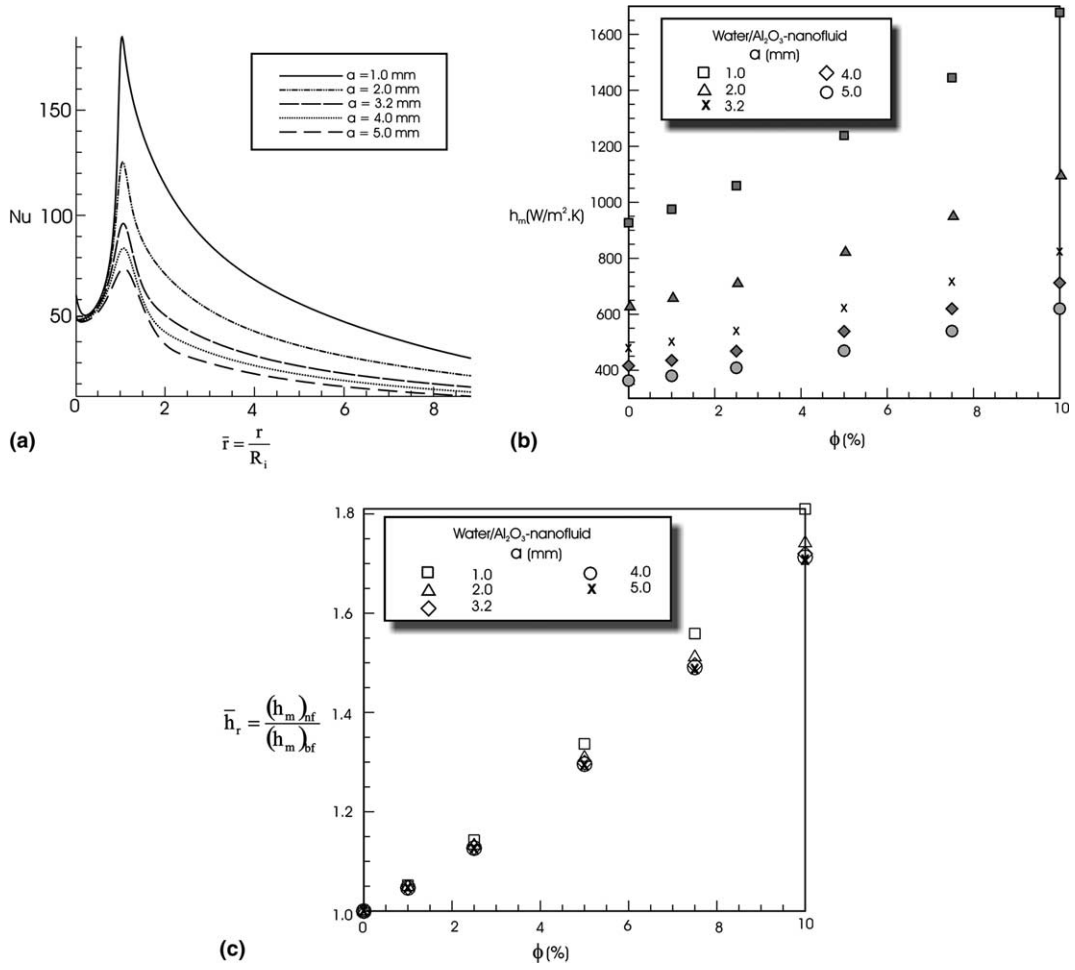

Fig. 11. Effect of distance separating disks in radial flow: (a) radial development of local Nusselt number, (b) averaged heat transfer coefficient and (c) averaged heat transfer coefficient ratio.

pronounced for smaller gap between disks. When these same results are presented in the relative form (i.e. normalised by the results as obtained for the base fluid for a same gap and *Re*), Fig. 11c, we can see that essentially the same distribution is found, with the exception of the case where $a = 1$ mm. Therefore, one can say that the distance separating the disks seems to have little effect on the global heat transfer benefit of the nanofluid when compared to the base fluid.

4.2.4. Effects of particle concentration on relative average wall shear stress

Although the use of nanofluids has beneficial heat transfer enhancement capabilities, it is to be expected that, because of their increased viscosity, they will also increase friction/pressure losses. Fig. 12 illustrates averaged wall shear stress ratio as a function of the nanoparticle volume fraction for the nanofluids considered (note that the quantities $\overline{\tau_{nf}}$ and $\overline{\tau_{bf}}$ are surface-averaged values that have been calculated over the entire area of the heated disk). As it can be seen, in both cases, considerable increases in wall shear stresses are found when the

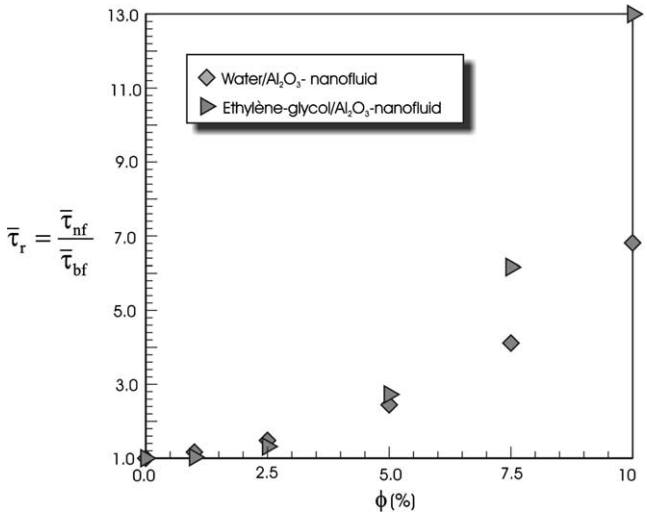

Fig. 12. Influence of parameter φ on relative average wall shear stress in radial flow.

particle volume fraction is increased. For example, for a 5% particle fraction of water–γAl_2O_3 nanofluid, a 2.5

fold increase in wall shear stress would be encountered. As was previously discussed, the Ethylene Glycol–γAl_2O_3 nanofluid was found to have the greatest increase in relative heat transfer capabilities. It is quite clear from Fig. 12 that the corresponding increases of the wall shear stresses are also quite important. Although the use of "slurry" type mixtures (i.e. mixtures with higher particle volume fractions) would probably have some practical applications, it remains to be seen what practical limits of particle volume fraction could be used in various applications. The benefits of the higher heat transfer rates versus the corresponding and drastic increases in viscosity would certainly have to be considered.

5. Conclusion

In this paper, we have investigated, by numerical simulation, the hydrodynamic and thermal characteristics of a laminar forced convection flow of nanofluids inside (a) a straight heated tube and (b) a radial space between coaxial and heated disks. Two particular nanofluids were considered, namely Ethylene Glycol–γAl_2O_3 and water–γAl_2O_3. Results have clearly revealed that the addition of nanoparticles has produced a remarkable increase of the heat transfer with respect to that of the base liquids. Such heat transfer enhancement that appears to be more pronounced with the increase of the particle volume concentration is accompanied, however, by a drastic adverse effect on the wall shear stress. It has been found that the Ethylene Glycol–γAl_2O_3 mixture yields, so far, a better heat transfer enhancement than water–γAl_2O_3. Unfortunately, it is also the one that has induced a more drastic and adverse effect on the wall shear stress. For the case of the tube flow in particular, results have also shown that, in general, the heat transfer enhancement due to nanoparticles clearly becomes more pronounced with an augmentation of the flow Reynolds number. For the two thermal boundary conditions considered, correlations have been provided in order to calculate the averaged Nusselt number of nanofluids in terms of the Reynolds and Prandtl numbers. On the other hand, for the case of a radial laminar flow and the range of the governing parameters studied, it has been found that both the through flow Reynolds number and the gap between disks seem to have insignificant effect on the heat transfer enhancement of nanofluids.

Acknowledgements

The authors wish to thank the Natural Sciences and Engineering Research Council of Canada, the "Ministère de l'Éducation du Québec" and the Faculty of the Graduate Studies and Research of the "Université de Moncton" for financial support to the present project. Thanks are also due to the Department of Mechanical Engineering of the "Université de Moncton" for allocating the computing facilities.

References

Ahuja, A.S., 1982. Thermal design of a heat exchanger employing laminar flow of particle suspensions. Int. J. Heat Mass Transfer 25 (5), 725–728.

Avila, R., Cervantes, J., 1995. Analysis of the heat transfer coefficient in a turbulent particle pipe flow. Int. J. Heat Mass Transfer 38 (11), 1923–1932.

Batchelor, G.K., 1977. The effect of Brownian motion on the bulk stress in a suspension of spherical particles. J. Fluid Mech. 83 (Pt. 1), 97–117.

Boothroyd, R.G., Haque, H., 1970. Fully developed heat transfer to a gaseous suspension of particles flowing turbulently in duct of different size. J. Mech. Eng. Sci. 12 (3), 191–200.

Brinkman, H.C., 1952. The viscosity of concentrated suspensions and solution. J. Chem. Phys. 20, 571–581.

Choi, S.U.-S., 1995. Enhancing thermal conductivity of fluids with nanoparticles. ASME Publications FED-vol. 231/MD-vol. 66, pp. 99–105.

Das, S.K., Putra, N., Thiesen, P., Roetzel, W., 2003. Temperature dependence of thermal conductivity enhancement for nanofluids. J. Heat Transfer 125, 567–574.

Drew, D.A., Passman, S.L., 1999. Theory of Multicomponent Fluids. Springer, Berlin.

Eastman, J.A., Choi, S.U.-S., Li, S., Soyez, G., Thompson, L.J., DiMelfi, R.J., 1999. Novel thermal properties of nanostructured materials. J. Metastable Nanocryst. Mater. 2 (6), 629–634.

Eastman, J.A., Choi, S.U.-S., Li, S., Yu, W., Thompson, L.J., 2001. Anomalously increase effective thermal conductivities of ethylene glycol-based nanofluids containing copper nanoparticles. Appl. Phys. Lett. 78 (6), 718–720.

Eckert, E.R.G., Drake Jr., R.M., 1972. Analysis of Heat and Mass Transfer. McGraw-Hill, New York, USA.

Gupte, S.K., Advani, S.G., Huq, P., 1995. Role of micro-convection due to non-affine motion of particles in a mono-disperse suspension. Int. J. Heat Mass Transfer 38 (16), 2945–2958.

Hamilton, R.L., Crosser, O.K., 1962. Thermal conductivity of heterogeneous two-component systems. I & EC Fundamentals 1 (3), 187–191.

Heaton, H.S., Reynolds, W.C., Kays, W.M., 1964. Heat transfer in annular passages simultaneous development of velocity and temperature fields in laminar flow. Int. J. Heat Mass Transfer 7 (7), 763–781.

Hornbeck, R.W., 1965. An all-numerical method for heat transfer in the inlet of a tube. ASME paper No. 65-WA/HT-36.

Jeffrey, D.J., 1973. Conduction through a random suspension of spheres. Proc. R. Soc. Lond., Series A 335, 355–367.

Keblinski, P., Phillpot, S.R., Choi, S.U.-S., Eastman, J.A., 2002. Mechanisms of heat flow in suspensions of nano-sized particles (nanofluids). Int. J. Heat Mass Transfer 45, 855–863.

Kurosaki, Y., Murasaki, T., 1986. Study on heat transfer mechanism of a gas–solid suspension impinging jet (effect of particle size and thermal properties). In: Proceedings of the 8th International Heat Transfer Conference, vol. 5, pp. 2587–2592.

Lee, S., Choi, S.U.S., 1996. Application of metallic nanoparticle suspensions in advanced cooling systems. ASME Publications PVP-vol. 342/MD-vol. 72, pp. 227–234.

Lee, S., Choi, S.U.-S., Li, S., Eastman, J.A., 1999. Measuring thermal conductivity of fluids containing oxide nanoparticles. J. Heat Transfer 121, 280–289.

Li, Q., Xuan, Y., 2002. Convective heat transfer performances of fluids with nano-particles. In: Proc. 12th Int. Heat Transfer Conference, Grenoble, France, pp. 483–488.

Maïga, S.E.B., 2004. Heat transfer of nanofluids in a uniformly heated tube (Étude numérique du tranfert thermique des 'nanofluides' dans un tuyau chauffé uniformément à la paroi). Master of Engineering Thesis, Faculty of Engineering, Université de Moncton, Moncton, NB, Canada, 96p.

Maïga, S.E.B., Nguyen, C.T., Galanis, N., Roy, G., 2004a. Heat transfer behaviours of nanofluids in a uniformly heated tube. Superlatt. Microstruct. 35 (3–6), 543–557.

Maïga, S.E.B., Nguyen, C.T., Galanis, N., Roy, G., 2004b. Heat transfer enhancement in forced convection laminar tube flow by using nanofluids. In: Proc. CHT-04 ICHMT Int. Symposium Advances Computational Heat Transfer, April 19–24 Norway, Paper No. CHT-04-101, 25p.

Masuda, H., Ebata, A., Teramae, K., Hishinuma, N., 1993. Alteration of thermal conductivity and viscosity of liquid by dispersing ultra-fine particles (dispersion of γ-Al_2O_3, SiO_2 and TiO_2 ultra-fine particles). Netsu Bussei (in Japanese) 4 (4), 227–233.

Maxwell, J.C., 1904. A Treatise on Electricity and Magnetism, second ed. Oxford University Press, Cambridge, pp. 435–441.

McGinn, J.H., 1956. Observations on the radial flow of water between fixed parallel plates. Appl. Sci. Res., Section A 5, 255–264.

Michaelides, E.E., 1986. Heat transfer in particulate flows. Int. J. Heat Mass Transfer 29 (2), 265–273.

Mochizuki, S., Yang, W.-J., 1986. Local heat transfer performance and mechanisms in radial flow between parallel disks. J. Thermophys. 1 (2), 112–115.

Murray, D.B., 1994. Local enhancement of heat transfer in a particulate cross flow—I. Heat transfer Mechanisms. Int. J. Multiphase Flow 20 (3), 493–504.

Nguyen, C.T., 1988. Convection mixte en régime laminaire dans un tuyau incliné soumis à un flux de chaleur constant à la paroi. Ph.D. thesis, Université de Sherbrooke, Québec, Canada.

Ohara, T., Suzuki, D., 2000. Intermolecular energy transfer at a solid–liquid interface. Microscale Thermophys. Eng. 4, 189–196.

Orfi, J., 1995. Convection mixte laminaire dans un tuyau incliné: développement simultané et phénomène de bifurcation. Ph.D. thesis, Université de Sherbrooke, Québec, Canada.

Pak, B.C., Cho, Y.I., 1998. Hydrodynamic and heat transfer study of dispersed fluids with submicron metallic oxide particles. Experiment. Heat Transfer 11 (2), 151–170.

Palm, S.J., 2004. Heat transfer enhancement by using nanofluids in a radial flow cooling system. Master of Engineering Thesis, Faculty of Engineering, Université de Moncton, Moncton, NB, Canada, in press.

Palm, S.J., Roy, G., Nguyen, C.T., 2004. Heat transfer enhancement in a radial flow cooling system using nanofluids. In: Proceedings of the CHT-04 ICHMT International Symposium on Advances Computational Heat Transfer, April 19–24 Norway, Paper No. CHT-04-121, 18p.

Patankar, S.V., 1980. Numerical Heat Transfer and Fluid Flow. Hemisphere Inc., McGraw-Hill, New York, NY, USA.

Petukhov, B.S., Polyakov, A.F., Strigin, B.K., 1969. Heat transfer in tubes with viscous-gravity flow. Heat Transfer—Sov. Res. 1 (1), 24–31.

Roy, G., Nguyen, C.T., Lajoie, P.-R., 2004. Numerical investigation of laminar flow and heat transfer in a radial flow cooling system with the use of nanofluids. Superlatt. Microstruct. 35 (3–6), 497–511.

Sato, Y., Deutsch, E., Simonin, O., 1998. Direct numerical simulation of heat transfer by solid particles suspended in homogeneous isotropic turbulence. Int. J. Heat Fluid Flow 19, 187–192.

Sohn, C.W., Chen, M.M., 1981. Microconvective thermal conductivity in disperse two-phase mixtures as observed in a low velocity Couette flow experiment. J. Heat Transfer 103, 45–51.

Szeri, A.Z., Schneider, S.J., Labbe, F., Kaufman, H.N., 1983. Flow between rotating disks, Part 1: Basic flow. J. Fluid Mech. 134, 103–131.

Wang, X., Xu, X., Choi, S.U.-S., 1999. Thermal conductivity of nanoparticles–fluid mixture. J. Thermophys. Heat Transfer 13 (4), 474–480.

Wang, B.-X., Zhou, L.-P., Peng, X.-F., 2003. A fractal model for predicting the effective thermal conductivity of liquid with suspension of nanoparticles. Int. J. Heat Mass Transfer 46, 2665–2672.

Warsi, Z.U.A., 1999. Fluid Dynamics Theoretical and Computational Approaches, second ed. CRC Press, Boca Raton, Florida, USA.

Xuan, Y., Li, Q., 2000. Heat transfer enhancement of nanofluids. Int. J. Heat Fluid Flow 21, 58–64.

Xuan, Y., Roetzel, W., 2000. Conceptions for heat transfer correlation of nanofluids. Int. J. Heat Mass Transfer 43, 3701–3707.

Xuan, Y., Li, Q., Hu, W., 2003. Aggregation structure and thermal conductivity of nanofluids. AIChE J. 49 (4), 1038–1043.